Non-oxidative Dehydrogenation of Ethane to Ethylene over ZSM-5 Zeolite Supported Iron Catalysts

Lu-Cun Wang[1,†], Yunya Zhang[1,2†], Jiayi Xu[3], Weijian Diao[2], Stavros Karakalos[2], Bin Liu[3], Xueyan Song[4], Dong Ding[1,*] Ting He[1]

[1] Biological and Chemical Processing Department, Idaho National Laboratory, Idaho Falls, ID 83401, USA

[2] Department of Chemical Engineering, University of South Carolina, Columbia, SC 29208, USA

[3] Department of Chemical Engineering, Kansas State University, Manhattan, Kansas 66506, United States

[4] Department of Mechanical and Aerospace Engineering, West Virginia University, Morgantown, WV 26506, USA

ABSTRACT

The non-oxidative dehydrogenation of ethane to ethylene on iron catalysts dispersed on ZSM-5 zeolite (Fe/ZSM-5) was investigated. Initial screening of various metal and metal oxide catalysts showed that the iron-based catalysts exhibited the best stability and the highest steady-state activity towards ethylene production under identical reaction conditions. The use of zeolite material as the support is critical for achieving optimal activity of iron catalysts, which gives much higher activity, by a factor of ~6 in terms of ethane conversion, than that on conventional γ-Al_2O_3 support. The activity of the Fe/ZSM-5 catalysts monotonically increases with the iron loading up to 10 wt%. The single-pass conversion of ethane can reach ~30% on the 10 wt% Fe/ZSM-5 catalyst with the selectivity to ethylene product exceeding 95%. Most prominently, the catalysts showed excellent stability with an activity loss of below 40% after 15 hours of reaction, while the Pt-based catalyst, despite its relatively higher initial activity, deactivated by over 90% during the first 2 hours on stream. In addition, the production rate of ethylene on the Fe/ZSM-5 catalyst can be further enhanced by lowering the total flow rate as well as by increasing the concentration of ethane in the feed gas. The as-prepared and spent Fe/ZSM-5 catalysts were systematically characterized along with density functional theory calculations to understand the origin of their excellent performances in the ethane dehydrogenation reaction.

KEYWORDS: non-oxidative ethane dehydrogenation, Fe/ZSM-5 catalyst, stability, deactivation, iron carbide

† Equal contribution

* Corresponding author, E-mail: dong.ding@inl.gov

1. INTRODUCTION

Ethylene is one of the most important building block petrochemicals produced in the United States and the world. The industrial-scale production of ethylene is conventionally practiced by steam cracking of ethane derived from crude oil, which is highly energy intensive requiring high temperature (>800 °C) and suffers from severe accumulation of carbon deposits on the reactor walls [1-3]. The shale gas revolution in the United States in recent years has resulted in an oversupply of ethane, the second major component of shale gas, and therefore significantly lowered its cost relative to crude oil. The emerging availability of ethane in shale gas as well as stranded gas reserves has stimulated enormous research interests in exploring alternative processes for ethylene production, particularly by catalytic ethane dehydrogenation via either oxidative or non-oxidative route [1-3].

Oxidative dehydrogenation (ODH) of ethane has been the subject of intensive research efforts in the past few decades [1, 3], due to its relatively higher single-pass conversions of ethane as well as the unnecessity of external energy input. However, the highly exothermic nature of the ODH process also brings about great challenges in heat recovery and process safety control. The tradeoff between ethane conversion and ethylene selectivity owing to the over-oxidation is another factor that hinders its commercial implementation. Additionally, the oxygen feed supply from air separation is also capital and energy intensive.

Non-oxidative ethane dehydrogenation (EDH), on the other hand, can avoid most of the issues associated with ODH but has the drawbacks of high energy demand, low single-pass conversion limited by the thermodynamic equilibrium, and oftentimes rapid coking-induced deactivation of the catalysts [2-3]. Potential solutions to these problems could be separation of H_2 product from the product mixture by applying membrane reactors so as to shift the reaction equilibrium toward ethylene formation [2] and developing highly selective and stable catalysts [3-7]. From a practical point of view, EDH process could be more attractive for the upgrading of ethane in stranded gases including flaring gas in shale oil field, refinery off-gas, shale gas in geographically disadvantaged locations, etc. [8] However, rather limited attention has been paid to EDH reaction in the literature in contrast to the numerous studies devoted to ODH of ethane.

Among various catalysts for non-oxidative dehydrogenation reactions, PtSn- and CrO_x-based catalysts are the most extensively studied and have been implemented industrially for propane dehydrogenation (PDH) to produce propylene [1-3, 9]. The support materials are typically Al_2O_3, or aluminates such as $MgAl_2O_4$ [1-2]. Other metal oxides, such as vanadium, gallium, zinc, and molybdenum oxides, have also been reported to show promising results, especially in the PDH reaction [3, 10-17]. As for the EDH reaction, Pt-based catalysts with promoters including Zn [18], Sn [4, 19], Ga [5-6], In [7], etc. have been investigated and shows either high activity or selectivity towards ethylene. Nevertheless, these catalysts usually undergo over 60% of activity loss during the first few hours of reaction due to coke formation accompanied by sintering of Pt particles [1-2, 4-5]. Therefore, the sought of alternative catalysts with both active and durable performance for EDH reaction still requires continuous research endeavors.

Supported iron oxides have been known to be excellent catalysts in ethylbenzene dehydrogenation for a long time, but they are usually regarded as poor catalysts for dehydrogenation of light alkanes [1, 20]. To our knowledge, iron oxide supported on zeolite as catalysts for EDH reaction under non-oxidative conditions have never been explored. In this work, we have, for the first time, shown that Fe/ZSM-5 can be used as highly efficient, selective and stable catalysts for EDH reaction. The catalytic performance of Fe/ZSM-5 could compete with or even surpass that of conventional Pt or metal oxides including Zn, Cr, Mo, Ga, V, etc., which have been well documented to be good catalysts for dehydrogenation of light alkanes. Various ZSM-5 and Al_2O_3 supported metal oxide catalysts were synthesized by the incipient wetness

impregnation method. The influence of iron loading and reaction parameters on the catalytic properties of Fe/ZSM-5 catalysts in EDH was investigated in detail. The textural, structural, and the surface properties of the as-prepared and used Fe/ZSM-5 catalysts were characterized using various techniques. The nature of active sites, reaction mechanism, and the origin of the deactivation behavior are discussed on the basis of the experimental results as well as DFT calculations.

2. EXPERIMENTAL SECTION

2.1. Preparation of catalysts

Two sets of ZSM-5 (CBV 5524G, Si/Al = 25, surface area 425 $m^2 \cdot g^{-1}$, Zeolyst International) supported catalysts were prepared by incipient wetness impregnation method. In the first catalyst set, different metal catalysts were obtained using aqueous solutions of zinc nitrate $Zn(NO_3)_2 \cdot 6H_2O$(Alpha Aesar, 99.9%), iron nitrate $Fe(NO_3)_2 \cdot 9H_2O$ (Alpha Aesar, 99.9%), gallium nitrate $Ga(NO_3)_3 \cdot 8H_2O$ (Alpha Aesar, 99.999%), Mo heptamolybdate $(NH_4)_6Mo_7O_{24} \cdot 4H_2O$ (Acros Organics, 99.9%), chromium nitrate $Cr(NO_3)_3 \cdot 9H_2O$ (Acros Organics, 99.9%), tetraammineplatinum(II) nitrate $Pt(NH_3)_4(NO_3)_2$ (Alpha Aesar, 99.9%) with the metal loading being kept constant at 2.0 wt%. In the second catalyst set, the Fe loading was varied at 0.5, 2.0 and 10 wt%. After impregnation, the catalysts were dried at room temperature in air overnight and further by ramping to 120 °C at 1 °C/min in flowing air (Airgas, Inc., ultrahigh purity) and holding at this temperature for 5 h. After drying, the samples were calcined in flowing air by ramping to 500 °C at 1 °C/min and holding at this temperature for 2 h.

The Al_2O_3 supported Fe catalyst was prepared by incipient wetness impregnation using aqueous iron nitrate and γ-Al_2O_3 (AEROXIDE Alu 130, surface area 130 $m^2 \cdot g^{-1}$). After impregnation, the catalysts were dried at 100 °C overnight followed by calcination in flowing air by ramping to 500 °C at 10 °C/min and holding at this temperature for 6 h.

2.2. Characterization

Textual properties of the supports and catalysts were measured with a Micromeritics ASAP 2020 analyzer by nitrogen adsorption at −196 °C. The samples were outgassed at 150 °C for 4 h before measurements. This instrument employed the Brunauer−Emmett−Teller (BET) method by measuring the quantity of nitrogen absorbed at −196 °C and the cumulative pore volumes and pore sizes were obtained by the Barrett−Joyner−Halenda (BJH) method from the desorption branches of the adsorption isotherms. The chemical composition of the samples was determined by an ICAP 6500 inductively coupled plasma optical emission spectrometer (ICP-OES).

Powder X-ray diffraction (XRD) measurements were performed with 2θ values between 20 and 60° by using a Rigaku Miniflex II diffractometer employing the graphite filtered Cu Kα radiation (λ = 1.5406 Å). The average crystallite sizes of Fe oxides were calculated from the diffraction peak at 35.71° by using the Scherrer equation: $D = K\lambda/(\beta\cos\theta)$, in which $K = 0.89$ is the Scherrer's constant, and β is the FWHM.

Diffuse reflectance UV–visible spectroscopy (DR UV–vis) characterization was carried out in a Cary 5000 UV-Vis-NIR spectrophotometer equipped with a Praying Mantis (TM) cell. Spectra were recorded at room temperature and in a wavelength range between 200 and 800 nm.

Transmission electron microscopy (TEM) was conducted to characterize the morphology of catalysts. Chemical analysis was carried out under TEM using energy dispersive X-ray Spectroscopy (EDS). The as-prepared samples were spread onto the Mo-grid for TEM imaging with a JEM-2100 transmission electron microscope at 200 kV. The used samples were dispersed in methanol and supported on carbon-film-coated copper grids before TEM images were recorded with a FEI Tecnai G2 F30 FEG STEM at an accelerating voltage of 300 kV.

NH_3-temperature programmed desorption (NH_3-TPD) experiments were carried out to analyze the acidic properties of the supports using a home-made apparatus. Prior to NH_3 adsorption, 100 mg sample was pretreated at 300 °C for 1 h under Ar stream (20 mL/min). After cooling to 100 °C, NH_3 was adsorbed using a flow of 10 vol % NH_3/N_2 (30 mL/min) for 0.5 h. The NH_3 desorption was performed in He (20 mL/min) with a heating rate of 10 °C/min and the NH_3 desorption profile was recorded with a mass spectrometer.

Thermal gravimetric analysis (TGA, STA449F3 NETZSCH Corp.) was used to investigate the carbon deposition of spent catalysts. The sample was preheated at 80 °C for 30 min in Ar (50 mL/min). Then the sample was heated to 780 °C at a rate of 10 °C/min in air (50 mL/min).

X-ray photoelectron spectroscopy (XPS) measurements were performed using a Kratos AXIS Ultra DLD XPS system with a monochromatic Al Ka source operated at 15 keV and 150W and a hemispherical energy analyzer. The X-rays were incident at an angle of 45° with respect to the surface normal. Analysis was performed at a pressure below 1×10^{-9} mbar. High resolution core level spectra were measured with a pass energy of 40 eV and analysis of the data was carried out using XPSPEAK41 software. The XPS experiments were performed while using an electron gun directed on the sample, for charge neutralization. The in-situ gas treatments of the catalysts were conducted in a catalysis cell attached to the XPS analysis chamber. All binding energies were referenced to the zeolitic Si 2p lines at 103.4 eV.

2.3. Catalyst testing

Catalytic tests were carried out at the atmospheric pressure in a quartz fixed-bed reactor with 7 mm inner diameter and 46 cm length. A mixture of 100 mg catalysts and 100 mg quartz sand with 50−70 mesh size distribution was loaded in the quartz tubular reactor. The temperature of the catalyst bed was measured by a thermocouple centered axially inside the reactor. Prior to the measurements, the catalysts were reduced at 610 °C in situ for 1 h in 10 vol.% H_2/Ar at a total flow of 60 mL/min. Afterwards, H_2/Ar was replaced by the reaction mixture of ethane (~9 vol.%) in Ar at a total flow of 60 mL/min. The product gas was analyzed by an online GC equipped with two flame ionization detectors (RTX-1 Pona column and Alumina Bond column). The overall ethane conversion was calculated according to Eq. (1):

$$X_{C2H6}\,(\%) = ([C_2H_6]_{in} - [C_2H_6]_{out})/\,[C_2H_6]_{in} \cdot 100\% \quad (1)$$

where $[C_2H_6]_{in}$, $[C_2H_6]_{out}$ are ethane concentration in the inlet and outlet gas flow. The relative selectivity to ethylene and methane was determined from Eqs. (2) and (3):

$$S_{C2H4,rel}\,(\%) = [C_2H_4]/([C_2H_4] + 0.5[CH_4]) \cdot 100\% \quad (2)$$

$$S_{CH4,rel}\,(\%) = 0.5[CH_4]/([C_2H_4] + 0.5[CH_4]) \cdot 100\% \quad (3)$$

The absolute selectivity to ethylene and methane was calculated using Eqs. (4) and (5):

$$S_{C2H4,abs}\,(\%) = [C_2H_4]/([C_2H_6] \times X_{C2H6}) \cdot 100\% \quad (4)$$

$$S_{CH4,abs}\,(\%) = 0.5[CH_4]/([C_2H_6] \times X_{C2H6}) \cdot 100\% \quad (5)$$

3. RESULTS

3.1. Catalytic performance in EDH Reaction

The ethane conversion and selectivity to ethylene for various metal and metal oxide catalysts supported on HZSM-5 are compared in Figure 1a and b, respectively, as a function of time on stream. Among all the catalysts tested, Pt/ZSM-5 exhibited the highest activity at time zero, with ca. 45% ethane conversion and 91% selectivity to ethylene. However, the Pt catalyst underwent rapid deactivation in the first 2 hours of reaction, losing almost 90% of its initial activity, and then continued to deactivate slowly. Concomitantly,

the selectivity to ethylene also rapidly decreased to 82% in 4 hours of reaction after initial rise up to 98%. Zn/ZSM-5 is the second most active catalyst in the series, with an initial ethane conversion of ca. 35% and selectivity to ethylene of 93%. Nevertheless, pronounced but relatively smoother deactivation also occurred for this catalyst, reaching an ethane conversion of 16% after 4 hours on stream. Unlike Pt/ZSM-5, the ethylene selectivity on Zn/ZSM-5 was almost constant at 96% after a slight initial increase from 93%.

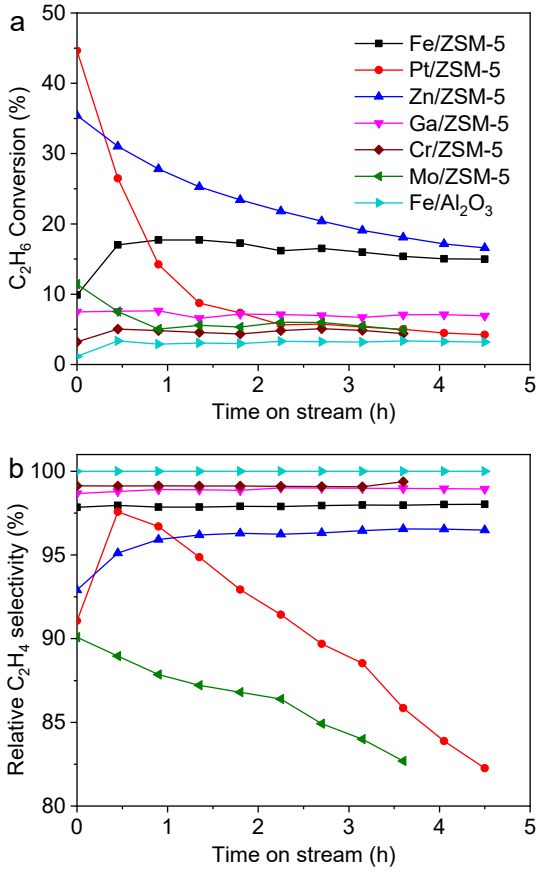

Figure 1. (a) C_2H_6 conversion and (b) C_2H_4 selectivity versus time on stream of various ZSM-5 and Al_2O_3 supported catalysts. Reactions conditions: 0.1 g catalyst, 9 vol.% C_2H_6/Ar, 60 mL/min, 600 °C.

In contrast to the above two catalysts, Fe/ZSM-5 showed a relatively lower initial ethane conversion of 10%. The activity, however, increased significantly by 70% to 17% in 30 min and then declined very slowly in the following 4 hours of reaction, with the steady-state activity being comparable to that of Zn/ZSM-5. The selectivity to ethylene on Fe/ZSM-5 was almost constant at 98%. Much lower activity was obtained on the other three ZSM-5 supported metal oxide catalysts, namely, Ga/ZSM-5, Cr/ZSM-5 and Mo/ZSM-5. These catalysts gave an ethane conversion of about 7% or less. The selectivity to ethylene was almost constant at 99% for Ga/ZSM-5 and Cr/ZSM-5 but much lower for Mo/ZSM-5 (90%) and deteriorated continuously. Note that negligible activity was obtained using the pristine ZSM-5 zeolite support. As far as the absolute selectivity of ethylene is concerned, the Fe/ZSM-5 catalyst had the highest and stable ethylene selectivity of ca. 70% among various catalysts tested (Figure S1).

The effect of different support material was also investigated on the Fe catalyst. Despite its high selectivity to ethylene (almost 100%), the Fe catalyst supported on γ-Al_2O_3 had an ethane conversion of only ca. 3% after reaction for 4 hours, by a factor of 5 lower than that supported on ZSM-5 zeolite.

Obviously, the type of support material had a remarkable influence on the catalytic performance of Fe catalysts for EDH reaction.

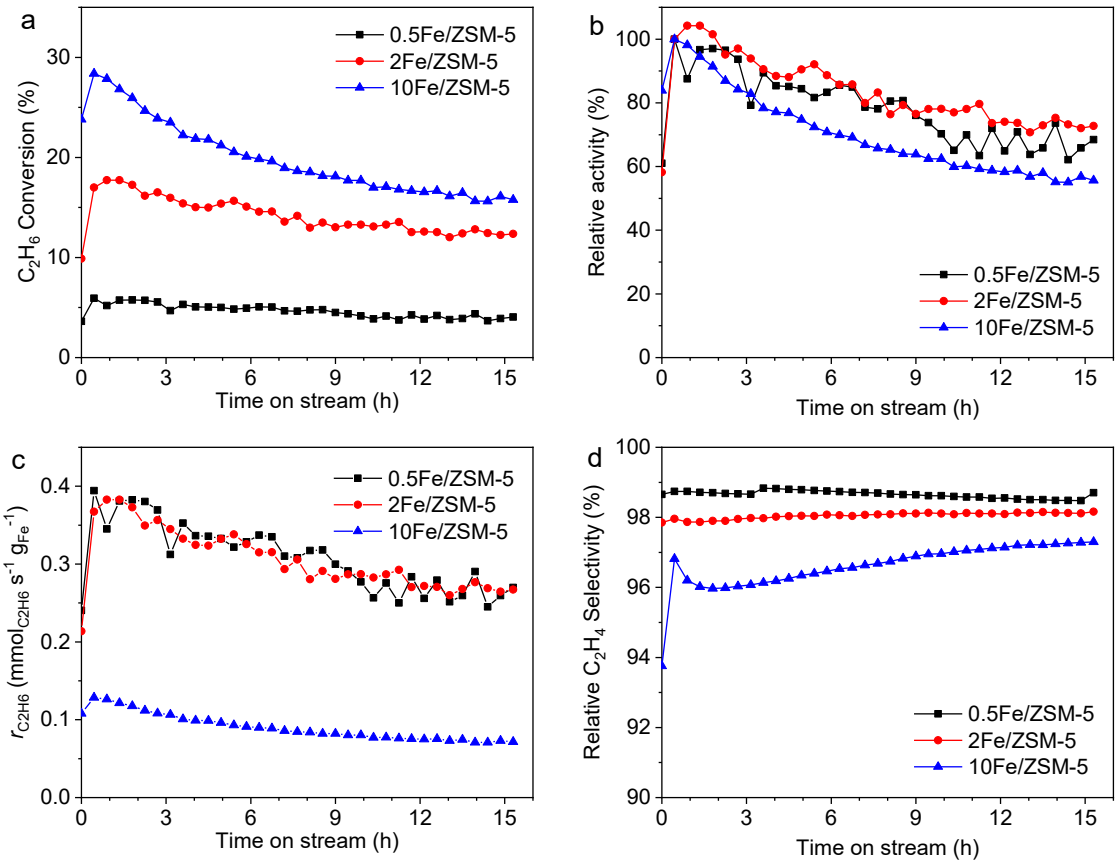

Figure 2. (a) C_2H_6 conversion, (b) Relative activity, (c) Fe-specific C_2H_6 reaction rate, and (d) C_2H_4 selectivity versus time on stream of Fe/ZSM-5 catalysts with varying Fe loadings. Reaction conditions: 0.1 g catalyst, 9 vol.% C_2H_6/Ar, 60 mL/min, 600 °C.

The effect of Fe loading on Fe/ZSM-5 catalysts was then investigated to optimize its catalytic performance (Figure 2). As the Fe content was raised from 0.5 wt% to 2 wt% and 10 wt%, the initial ethane conversion at time 30 min steadily increased to 6%, 17% and 28% (Figure 2a), respectively. After 15 h under reaction conditions, the ethane conversion decreased to 4%, 12% and 16% (Figure 2a), corresponding to a loss of activity by 31%, 27%, and 44% (Figure 2b), respectively. The reaction rate of ethane normalized by Fe content was almost the same for 0.5 and 2Fe/ZSM-5 but significantly higher by a factor of 4 than that of 10Fe/ZSM-5 (Figure 2c). In addition, there were only small changes (< 2%) in the relative selectivity of ethylene for 0.5Fe/ZSM-5 and 2Fe/ZSM-5 with reaction time. The ethylene selectivity on 10Fe/ZSM-5, in contrast, rapidly increased in the first 30 min of reaction and then decreased after a maximum, followed by a steady increase up to 97% after 15 h of reaction (Figure 2d). A similar trend was obtained for the absolute selectivity of ethylene, which dramatically increased from 18% to 66% in the first 30 min and then became stable at around 70% (Figure S2). Overall, it is clear that higher Fe loading led to better catalytic activity of the Fe/ZSM-5 catalyst but relatively faster deactivation as well as slightly lower selectivity to ethylene.

As expected from the strong endothermic nature of EDH reaction, the temperature had significant influence on the reactivity of the Fe/ZSM-5 catalyst (Figure 3). With the temperature rise from 450 °C to

650 °C, the ethane conversion on the 0.5, 2 and 10Fe/ZSM-5 catalysts increased almost exponentially from ca. 1% to 12%, 41%, and 52%, respectively (Figure 3). The linear Arrhenius plot based on the rate of C_2H_4 formation for each catalyst (Figure 3b) gave a comparable apparent activation energy (E_a) of 170±5, 177±13, and 163±10 kJ·mol^{-1} for the 0.5, 2 and 10Fe/ZSM-5 catalysts, respectively. Previously, a similar E_a for ethane dehydrogenation, 163 kJ·mol^{-1}, was obtained on Ga_2O_3/HAlMFI catalyst [21]. Note that these values are relatively greater than that obtained from Pt-based catalysts for EDH reaction. For instance, the E_a for ethane dehydrogenation over Pt/Mg(Al)O and PtSn/Mg(Al)O catalysts was reported to be 114 kJ·mol^{-1} and 102 kJ·mol^{-1}, respectively [4]. In another study, the E_a was determined to be 72±4 kJ mol^{-1} for Pt/SiO_2 and 99±5 kJ mol^{-1} for $PtZn/SiO_2$ [18].

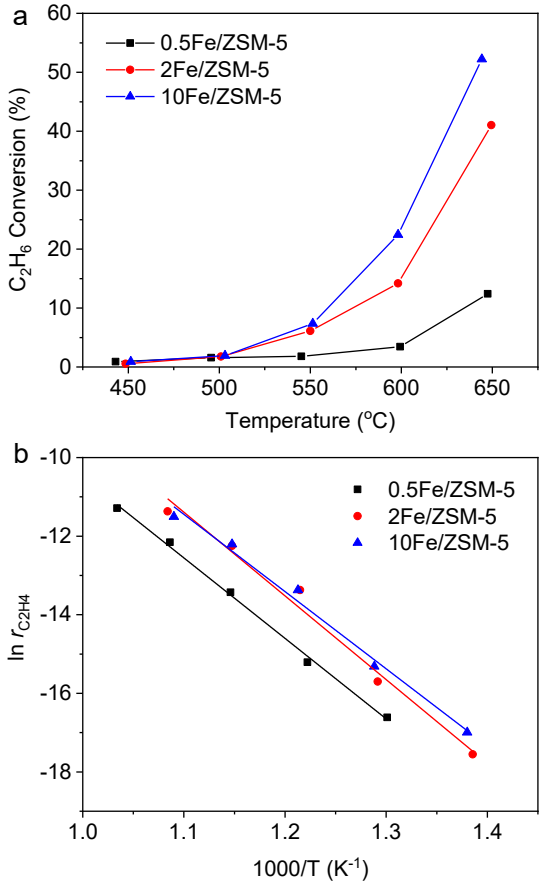

Figure 3. (a) C_2H_6 conversion as a function of reaction temperature. Reaction conditions: 0.1 g catalyst, 9 vol.% C_2H_6/Ar, 60 mL/min. (b) Arrhenius plots of Fe/ZSM-5 catalysts.

Apart from the temperature, several additional parameters that could affect the catalytic performance were investigated in detail on the catalyst 2Fe/ZSM-5 when the steady state was reached after 15 h on stream. Figure 4 shows the effect of adding H_2 to the feed on the activity and selectivity. By raising the H_2/C_2H_6 ratio from 0.25 to 2.5 the steady-state activity in ethylene formation of the 2Fe/ZSM-5 catalyst decreased by ca. 40% from 2.1 to 1.2 µmol·s^{-1}·g_{cat}^{-1}. Meanwhile, H_2 addition to the feed caused a slight increase in the formation rate of methane, resulting in an increase in the selectivity of methane by a factor of 2 (Figure 4b). Similar effect of H_2 addition on the activity and selectivity in EDH reaction has also been reported on the PtSn/Mg(Al)O catalyst [4].

Extending the residence time or lowering the flow rate of ethane could significantly boost the activity of ethylene production on 2Fe/ZSM-5 (Figure 5). The rate of ethylene formation increased by a factor of 6 as the W/F increased from 0.08 to 0.6 $g_{cat} \cdot s \cdot mL^{-1}$. However, longer residence time also promoted the production rate of methane by a factor of 23 (Figure 5a), thus leading to lower relative selectivity to ethylene (Figure 5b). The impact of residence time on the activity and selectivity of Fe/ZSM-5 for EDH reaction is in common with that on the Pt-based catalysts [4]. It has been suggested that methane may be formed both as a primary product of ethane hydrogenolysis and as a secondary product of ethylene hydrogenolysis [4].

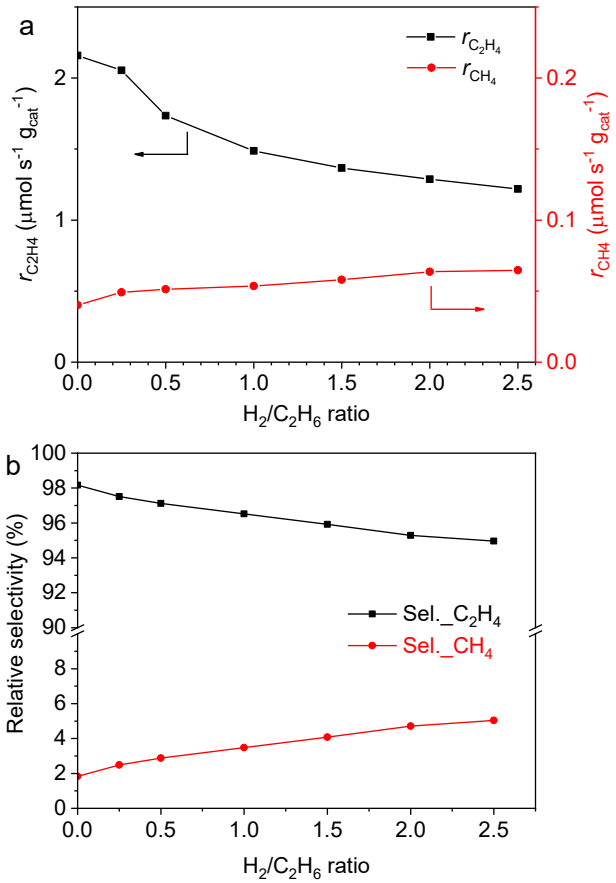

Figure 4. Effect of H_2/C_2H_6 ratio on the (a) C_2H_4 and CH_4 production rate and (b) selectivity on 2Fe/ZSM-5. Reaction conditions: 0.1 g catalyst, 9 vol.% C_2H_6/Ar, 60 mL/min, 600°C.

The effects of ethane concentration on the performance of 2Fe/ZSM-5 are shown in Figure 6. The production of ethylene increased almost linearly with the ethane concentration in the feed. Similar trend was also obtained for methane formation rate as function of ethane concentration. On the other hand, the selectivity to ethylene relative to methane only slightly declined from 98% to 95% as the concentration of ethane increased from 2 vol% to 100 vol%. It should be noted, however, that in addition to the major product ethylene and methane, higher hydrocarbon products were also detected and became more significant at higher ethane concentration, including propylene, butylene, and even aromatics such as benzene and toluene. The absolute selectivity to these byproducts estimated on the basis of total ethane conversion amounts to ca. 50% when pure ethane was used as the feed. This result is not surprising considering the existence of acid sites on the ZSM-5 zeolite support which could catalyze consecutive

transformations of the ethylene product including hydrogenolysis, cracking, oligmerization, isomerization, alkylation, etc. [22-23].

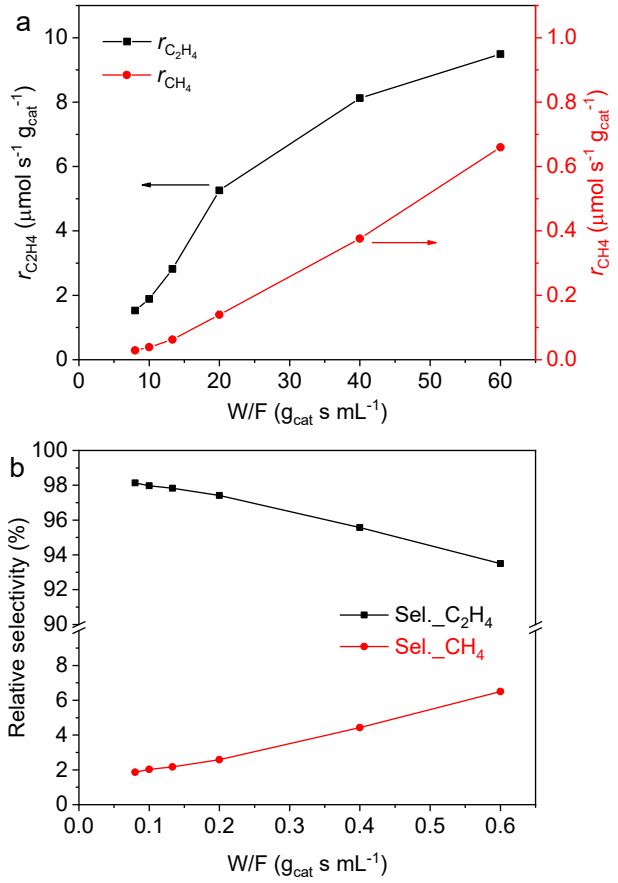

Figure 5. Effect of W/F on the (a) C_2H_4 and CH_4 production rate and (b) selectivity on 2Fe/ZSM-5. Reaction conditions: 100 mg catalyst, 9 vol.% C_2H_6/Ar, 60 mL/min, 600°C.

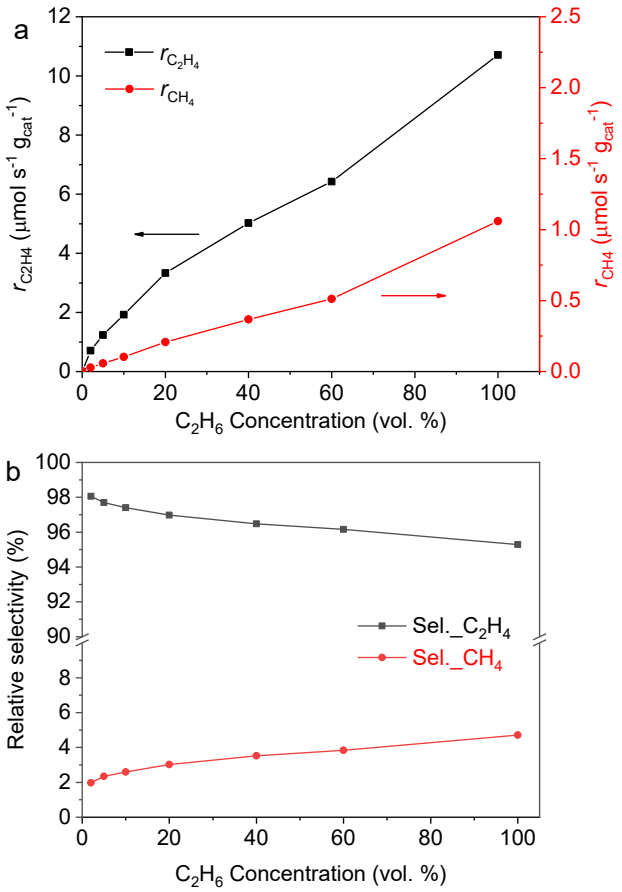

Figure 6. Effect of C_2H_6 concentration on the (a) C_2H_4 and CH_4 production rate and (b) selectivity on 2Fe/ZSM-5. Reaction conditions: 0.1 g catalyst, 60 mL/min, 600°C.

3.2. Characterization of As-prepared Fe/ZSM-5 Catalysts

The physical properties of various Fe/ZSM-5 catalysts are reported in Table 1. The actual Fe content for each Fe/ZSM-5 catalyst measured by ICP-OES analysis is close to the nominal value. The introduction of Fe caused a moderate decrease in the specific surface area to 393 $m^2 \cdot g^{-1}$ and 352 $m^2 \cdot g^{-1}$ for 0.5Fe/ZSM-5 and 2Fe/ZSM-5, respectively, compared with that of the pristine ZSM-5 zeolite (425 $m^2 \cdot g^{-1}$). Nevertheless, further raising the Fe loading by a factor of 5 to 10 wt% only resulted in a slight decrease to 345 $m^2 \cdot g^{-1}$. In addition, there were essentially no significant changes in the pore volumes of Fe/ZSM-5 catalysts with different Fe loadings (Table 1).

Table 1. Physical Properties of Fe/ZSM-5 Catalysts

Catalyst	Fe loading[a] (wt%)	S_{BET} ($m^2 \cdot g^{-1}$)	V_{total}[b] (cm^3/g)	V_{micro}[c] (cm^3/g)	d_{Fe}[d] (nm)	Acid site density[e] ($\mu mol_{NH3} \cdot g_{cat}^{-1}$)
0.5Fe/ZSM-5	0.61	393	0.30	0.16	<3 (-)	
2Fe/ZSM-5	1.9	352	0.26	0.14	<3 (-)	
10Fe/ZSM-5	9.0	345	0.29	0.18	21.5 (23.9)	

[a] Determined by ICP-OES analysis. [b] total pore volume. [c] volume of micropores. [d] particle size of iron oxide determined by TEM, values in the parenthesis are estimated from XRD data. [e] Determined by NH_3-TPD.

The XRD patterns of as-prepared Fe/ZSM-5 catalysts showed the typical diffraction peaks of MFI-type structure (Figure 7a), indicating that the crystalline nature of zeolites was maintained without any structural change upon the addition of Fe. No discernable diffraction peaks characteristic of iron phases could be seen from 0.5Fe/ZSM-5 and 2Fe/ZSM-5, suggesting that Fe species should be highly dispersed on the zeolite surface. As the Fe loading increased to 10 wt%, additional diffraction peaks at 2θ = 33.2°, 35.7°, and 53.6° emerged and could be ascribed to a-Fe_2O_3 phase [24-26]. Apparently, growth in crystallite size of Fe oxide occurred at high Fe loading. By using the Scherrer equation the average crystallite size of Fe oxide on 10Fe/ZSM-5 was estimated to be ca. 23.9 nm.

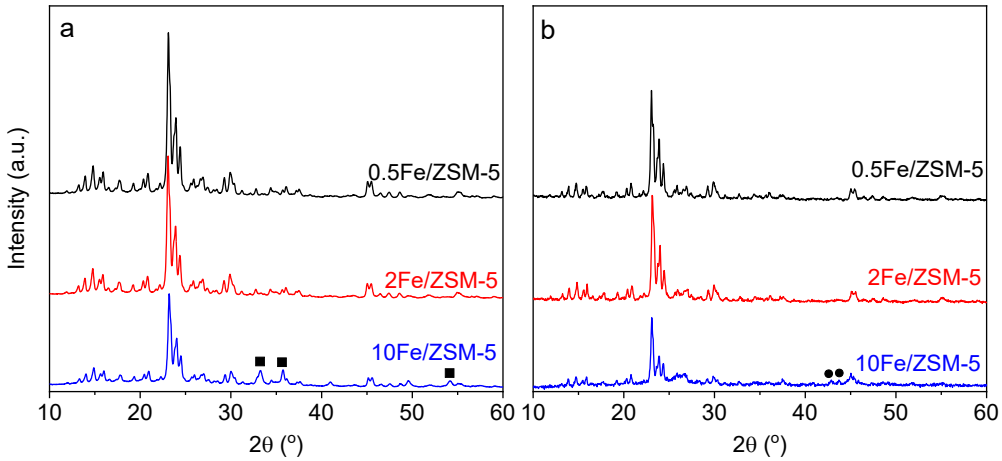

Figure 7. XRD patterns of Fe/ZSM-5 catalysts (a) before and (b) after reaction. (■) α-Fe_2O_3, (●) Fe_3C.

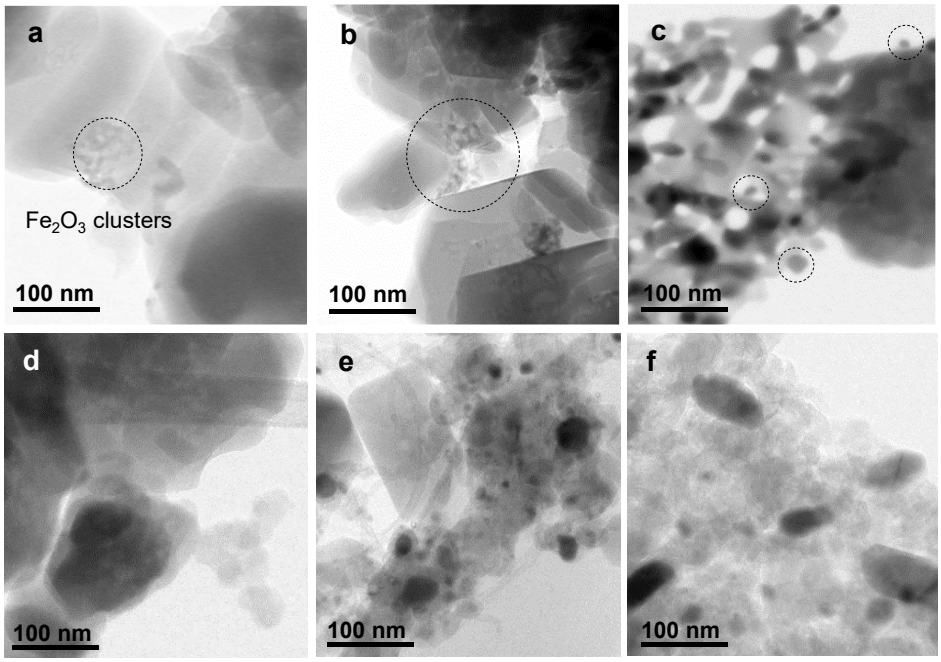

Figure 8. Representative TEM images of Fe/ZSM-5 catalysts before reaction (upper panel) and after reaction for 15 h (lower panel). (a,d) 0.5Fe/ZSM-5 (b,e) 2Fe/ZSM-5 and (c,f) 10Fe/ZSM-5.

`

The morphology and the crystallite size of Fe oxides on the fresh Fe/ZSM-5 catalysts were also examined by TEM (Figure 8). Small aggregated Fe oxide clusters in size of <3 nm can be resolved in the porous zeolite matrix on 0.5Fe/ZSM-5 and 2Fe/ZSM-5 (Figures 8a and 8b). Fe oxide nanoparticles became distinct on 10Fe/ZSM-5, with an average particle size of 21.5 nm (Figure 8c), in good agreement with the XRD result. Note that while the zeolite particles in 0.5 and 2Fe/ZSM-5 were present in the shape of large patches with an average diameter of hundreds of nanometers, part of the zeolite support in 10Fe/ZSM-5 seemed to have much smaller crystallite size and irregular shapes. This discrepancy is consistent with the relatively weaker diffraction intensity in the XRD pattern of 10Fe/ZSM-5 (Figure 7a), suggesting that high Fe loading could change the structure of the zeolite support, probably resulting from the strong interaction between iron oxide and the zeolite support.

The Fe 2p XPS spectra of all three as-prepared Fe/ZSM-5 samples comprised two components at BE of ~710.5 eV (Fe $2p_{3/2}$) and ~723.7 eV (Fe $2p_{1/2}$), respectively, with a spin–orbit coupling energy gap of ca. 13.6 eV (Figure 9a). Both of these peaks are accompanied by distinct satellite peaks at around 718.4 and 732.6 eV. These features are characteristic of Fe oxides [24, 27-29]. A deconvolution analysis of the spectra revealed the existence of both Fe^{3+} (711.7 eV) and Fe^{2+} (709.6 eV) species on the surface of all three Fe/ZSM-5 samples. The presence of Fe^{2+} on 10Fe/ZSM-5 may result from surface reduction under the ultrahigh vacuum conditions and X-ray flux of the measurement [29]. The surface atomic concentration of Si, Al, C, and O determined from the corresponding peak intensity was comparable for all three samples, except for the increasing Fe content (Table 2).

3.3. Characterization of Fe/ZSM-5 Catalysts After Reaction

As compared with that of the fresh samples, the intensity of the diffraction peaks of ZSM-5 zeolite was slightly weaker for 0.5Fe/ZSM-5 and 2Fe/ZSM-5 after reaction for 15 h (Figure 7b). In contrast, the XRD pattern of 10Fe/ZSM-5 showed significantly declined intensity, probably related to partial breakdown of the crystalline structure of the zeolite support under harsh reaction conditions and/or severe accumulation of carbon deposits on the catalyst surface (see TEM results below). No diffraction peaks from reduced iron oxides, metallic iron, or iron carbides could be identified from the XRD patterns of 0.5Fe/ZSM-5 and 2Fe/ZSM-5. However, additional weak diffraction peaks at 42.9° and 43.7° appeared in the XRD pattern of 10Fe/ZSM-5. Similar results have been reported previously for Fe/ZSM-5 catalysts when subject to methane decomposition or aromatization reactions for a certain period of time and these peaks were assigned to Fe_3C (cementite) [24, 26]. It has been suggested that Fe_2O_3 in the fresh catalyst would be reduced and carburized stepwise under reaction conditions, i.e., $Fe_2O_3 \rightarrow \alpha$-Fe metal$\rightarrow Fe_3C$.

TEM results showed that the morphology of 0.5Fe/ZSM-5 was only slightly affected after reaction (Figure 8d), whereas large Fe particles resulting from the growth of Fe clusters could be clearly seen from the TEM images for the used 2Fe/ZSM-5 (Figure 8e) and 10Fe/ZSM-5 (Figure 8f). The sizes of Fe particles in both 2Fe/ZSM-5 and 10Fe/ZSM-5 exhibited a broad distribution in the range of a few nanometers to ca. 50 nm. Note that despite the marked degree of particle growth in the used 2Fe/ZSM-5, no reflections associated with Fe or Fe oxide crystallites were detected by XRD. This is likely due to the relatively low amount of Fe loading. In addition, high-resolution TEM images combined with EDX analysis clearly showed that the Fe nanoparticles were encapsulated in thick layers of carbon species (up to ca. 10 nm thick, see also Figures S3 and S4). In addition to carbon layers on Fe particles, other carbon structures such as nanotubes, chains were also observed on the used 2Fe/ZSM-5 (Figure 8e and S3). Elemental analysis by EDX indicates that carbon deposits also existed on the zeolite support (see Figure S5).

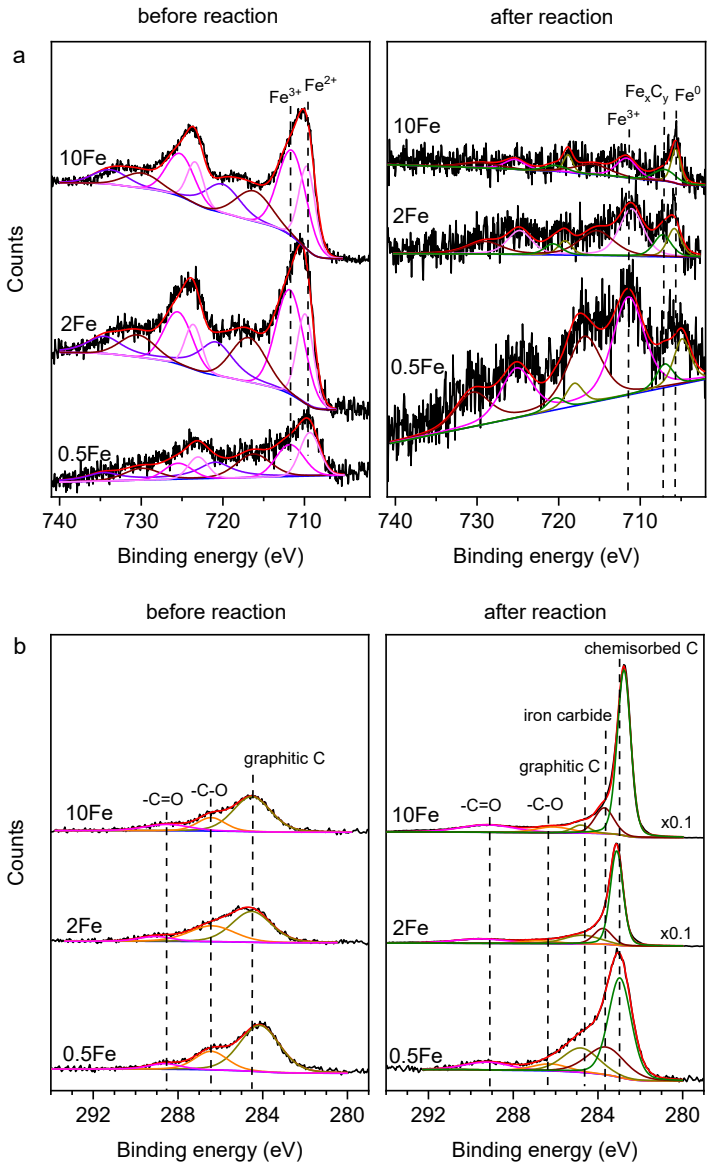

Figure 9. (a) Fe2p and (b) C1s XPS spectra of Fe/ZSM-5 catalysts before and after reaction.

Table 2 Surface atomic concentration of Fe/ZSM-5 catalysts determined by XPS before and after reaction.

Catalyst		Atomic concentration (at.%)					
		Fe	C	Si	Al	O	Si/Al ratio
0.5Fe/ZSM-5	Fresh	0.6	6.7	26.8	1.5	63.4	18
	Used	0.4	10.0	25.4	1.6	62.6	16
2Fe/ZSM-5	Fresh	1.4	4.6	26.9	1.5	64.7	18
	Used	0.5	45.0	16.3	1.0	37.2	16
10Fe/ZSM-5	Fresh	6.3	5.6	24.5	1.2	61.6	20
	Used	0.5	88.4	3.1	0.3	7.7	10

The amount of deposited carbon on the spent Fe/ZSM-5 catalysts was quantitatively analyzed by TGA in an oxidizing atmosphere. From the weight loss profiles (Figure 10) the amount of weight loss due to coke combustion was determined to be 0.005, 0.049, and 0.17 $g \cdot g_{cat}^{-1}$ for 0.5Fe/ZSM-5, 2Fe/ZSM-5, and 10Fe/ZSM-5, respectively. The corresponding value would be 0.82, 2.56, 1.91 $g \cdot g_{Fe}^{-1}$, respectively, if normalized to the Fe loading. Apparently, higher Fe loading on the zeolite support accounts for, at least in part, the higher amount of coke deposits under the same reaction conditions. The different acidity of the Fe/ZSM-5 catalysts may also play a role in the coke formation since it is well known that acid sites on zeolite can promote side reactions such as isomerization, cyclization and coking during alkane dehydrogenation [22-23].

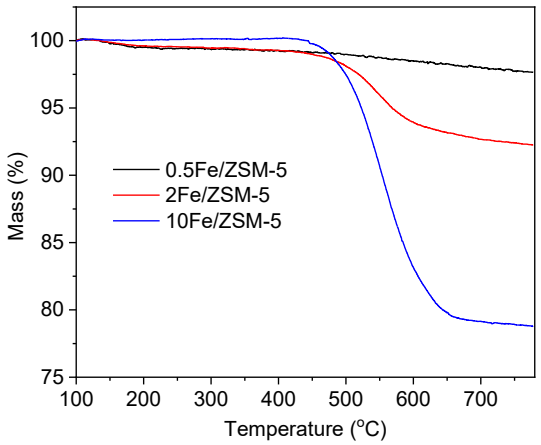

Figure 10. TGA profiles of Fe/ZSM-5 catalysts with varying Fe loadings after reaction for 15 h.

The Fe/ZSM-5 catalysts after exposure to EDH reaction conditions were also investigated by XPS (Figure 9). It should be noted that the catalysts were transferred immediately to the analysis chamber after pretreatments in the attached reaction chamber without exposure to air in between; therefore, the information obtained thereby should reflect the surface chemical states of the catalysts under in-situ conditions. The Fe 2p XPS spectra became rather weak after reaction for all samples (Figure 9a), especially for 2Fe/ZSM-5 and 10Fe/ZSM-5, mainly due to the coverage of Fe particles by large amount of carbon species, as shown by the TEM results above. The main characteristic feature of Fe^{3+} species could still be identified after reaction. In addition to the signals from oxidic Fe species, two new peak emerged at BE of 707.1 eV and 705.5 eV, which could be ascribed to the formation of carbide species and metallic Fe^0 [24, 29-30], respectively.

The C 1s spectra for the Fe/ZSM-5 catalysts after reaction are composed of at least five peaks, with the one at ~ 283 eV being most prominent (Figure 9b). In accord with the TGA results, the C1s peak intensities of both 2Fe/ZSM-5 and 10Fe/ZSM-5 were significantly stronger, by at least an order of magnitude, than that on 0.5Fe/ZSM-5. According to the literature [24, 31-33], the peaks at ~283.0, 283.7, 284.8, and 286.2 eV could be attributed to the signals from chemisorbed carbon, iron carbide, graphitic carbon, and hydrocarbon C–C bonds, respectively. The broad peak centered at ca. 289.2 eV could be assigned to –C=O double bond.

The surface atomic concentration determined from the XPS data for 0.5Fe/ZSM-5 catalyst only slightly changed after reaction. In contrast, there was a significant decrease in the surface concentration of all elements except for carbon on 2Fe/ZSM-5 and 10Fe/ZSM-5. Note that the surface Si/Al ratio decreased

most significantly from 20 on the as-prepared 10Fe/ZSM-5 to 10 after reaction (Table 2). It is possible that reaction-induced dealumination occurred for 10Fe/ZSM-5 leading to relative enrichment of Al on the surface.

4. DISCUSSION

4.1. Nature of Active Sites on Fe/ZSM-5 for EDH Reaction

Kinetic experiments resulted in comparable apparent E_a within the experimental error on the three Fe/ZSM-5 catalysts for EDH reaction, reflecting that different Fe loadings do not change the reaction mechanism. Most likely, the nature of active sites for EDH reaction remained the same for different Fe/ZSM-5 catalysts. Accordingly, the reaction rate per active site should be constant over different Fe/ZSM-5 catalysts under the same reaction conditions. In line with this postulation, the Fe-normalized reaction rate of ethane was almost identical on 0.5Fe/ZSM-5 and 2Fe/ZSM-5 (see Figure 2c). Nevertheless, the value was by a factor of 3 lower for 10Fe/ZSM-5. This may be rationalized by the fact that the amount of active Fe species on 10Fe/ZSM-5 was overestimated due to the presence of large Fe oxide particles, since the reaction rate was calculated by taking into account the total amount of Fe instead of the surface Fe only. In contrast, the active Fe species were well dispersed when the Fe loading is below 2 wt%, as evidenced by the absence of crystalline Fe_2O_3 in either 0.5Fe/ZSM-5 or 2Fe/ZSM-5.

The Fe/ZSM-5 catalysts initially showed a rapid increase in ethane conversion to different extents before reaching a maximum in an hour of reaction (see Figure 2a). On 10Fe/ZSM-5, concomitant with the activity enhancement, there was also an improvement in the selectivity to ethylene, with a dramatic increase from ~18% to ~70% (see Figure S2). This behavior may be induced by the structure transformation in the as-prepared Fe/ZSM-5 catalysts upon exposure to reaction conditions, leading to the generation of intrinsically more active and selective sites for EDH reaction. This presumption is supported by the XPS results of the used Fe/ZSM-5 catalysts, which clearly showed that the iron oxides underwent partial reduction and carburization after reaction. Quantitative analysis revealed that the reduced and carburized Fe species amounted to ca. 38% of the total surface Fe species on 0.5Fe/ZSM-5 and 2Fe/ZSM-5 after reaction, whereas this value was ca. 60% for 10Fe/ZSM-5. Since the *in situ* XPS data was collected after reaction for 60 min, the results clearly indicate that both metallic Fe and Fe carbides were already formed at 60 min of time on stream, where the catalyst reached a maximum activity for the EDH reaction (see Figure 2a). Therefore, it is very likely that both metallic Fe and Fe carbides are catalytically active species for the ethane activation. Moreover, the XRD pattern of 10Fe/ZSM-5 after reaction for 15 h indicated the presence of only carburized Fe species in the bulk phase although the existence of metallic Fe could not be excluded considering the detection limit of XRD technique. Accordingly, we speculate that the extent of Fe carburization may increase with extended reaction time. Similar evolution of Fe species from Fe metal to Fe carbide with reaction time for hours has been reported recently for Fe/ZSM-5 catalysts in non-oxidative aromatization of methane [24].

In order to further understand the dehydrogenation mechanism of ethane and discriminate the different possible active sites on Fe/ZSM-5 catalysts, DFT calculation was performed on three model catalysts (Figure S7), representing iron oxide, metallic iron, and iron carbide supported on ZSM-5 zeolite (Figure S8 and Figure S9). Figure S3 also indicates that both Fe metal and Fe carbide are both active sites for the EDH reaction, in line with the experimental results discussed above. The results showed that C_2H_4 desorption from metallic iron metal and Fe_2C is energy demanding, requiring about 2 eV (Figure S9). Interestingly, the apparent activation energy measured on these catalysts is about 1.7 ~ 1.8 eV, which is close to the DFT calculations and likely to be a rate-limiting step. It should be pointed out, however, that C_2H_4 desorption from Fe metal (~2 eV) is relatively more difficult than that from the Fe_2C surface (~1.25 eV). In addition, the carburization of Fe metal associated with C_2H_4 decomposition is energetically more

favorable compared with the direct C_2H_4 desorption from Fe metal. This result is in accord with the observation that Fe_3C but no Fe metal was detected by XRD after reaction for 15 h, which suggests that Fe metal, after being formed initially, will gradually be carburized with time. This may also explain the improved selectivity of C_2H_4 relative to CH_4 with extended reaction time, especially on the 10Fe/ZSM-5 catalyst (see Figure 2d).

DFT calculations also show that reaction of ethane over iron oxide, forming H_2O, C_2H_4 and reduced iron species (as in -Fe_2O-) is a energetically favored pathway (Figure S9). Hence, considering the reductive and non-oxidative environment under reaction conditions, Fe^{3+} would likely be reduced and transformed to lower oxidation states or carbides shortly without external oxygen sources.

4.2. Reaction Mechanism of EDH Reaction on Fe/ZSM-5 Catalysts

The elementary processes involved in EDH reaction to produce ethylene, could be described by the following reaction steps:

1) $C_2H_6 + 2^* \rightarrow C_2H_5^* + H^*$
2) $C_2H_5^* + 2^* \rightarrow C_2H_4^{**} + H^*$
3) $C_2H_4^{**} \rightleftharpoons C_2H_4 + 2^*$

The formation of byproducts including methane and carbon is proposed to proceed via consecutive reaction of adsorbed ethylene:

4) $C_2H_4^{**} \rightleftharpoons CH_3CH^{**}$
5) $CH_3CH^{**} \rightarrow \rightarrow \rightarrow CH_3^* + H^* + C$
6) $CH_3^* + H^* \rightarrow CH_4 + 2^*$

Previous studies on Pt-based catalysts for EDH reaction [4] have reported that the presence of H_2, within a certain limit of partial pressure, had a promotional effect on the formation rate of ethylene, which suggested that secondary dehydrogenation of adsorbed $C_2H_5^*$ to form ethylene could be assisted by adsorbed H atoms. This effect, however, was not observed in our case. Based on the proposed mechanism, the addition of H_2 in the reaction mixture would apparently promote the rate of Reaction 1 and 2 in the reverse direction, leading to the decreased formation rate of ethylene (Figure 4). In addition, the concomitant increase in methane formation rate suggests that higher H_2 partial pressure will facilitate Reaction 6 in the forward direction.

While both the formation rate of ethylene and methane increased significantly by prolonging the residence time and by raising the ethane concentration in the reaction mixture, the corresponding selectivity of ethylene decreased monotonously relative to that of methane (see Figures 5 and 6). It can be expected that both the longer residence time and higher ethane concentration will result in higher surface coverage of activated ethane or adsorbed $C_2H_5^*$ intermediates, which will boost the rates of both Reaction 3 and 4, thus leading to higher rates of ethylene formation and its transformation into methane and carbon products. On the other hand, based on Reaction 1 and 2, the formation of one adsorbed ethylene molecule is accompanied by the generation of two adsorbed H atoms. Accordingly, the accumulation rate of surface adsorbed H atoms would be two times of that for ethylene. The larger extent of increase in surface H coverage will accelerate Reaction 6 and consequently shift the reaction equilibrium of adsorbed ethylene toward ethylidene formation (Reaction 4). As a result, the selectivity to methane will increase as a function of residence time and ethane concentration.

4.3. Deactivation of Fe/ZSM-5 Catalysts in EDH reaction

Coke deposition has been regarded as the main cause for the deactivation of catalysts in alkane dehydrogenation reactions [1-3, 8, 34]. In this study, although the Fe/ZSM-5 catalysts exhibited excellent stability as compared with other highly active catalysts, including Zn- and Pt-based ones, there was still deactivation by up to 40% relative to the maximum activity after reaction for 15 h (see Figure 2b). Characterization by TGA, XPS, and TEM of the spent catalysts confirmed the accumulation of carbon species on all Fe/ZSM-5 catalysts investigated and the amount of carbon deposits appeared to scale with the Fe content. In an attempt to regenerate the catalyst after reaction for 15 h, we have treated the used 2Fe/ZSM-5 catalyst *in situ* by flowing air at 610 °C for 1 h and subsequently switched back to the reaction conditions. The results showed that the regeneration treatment had negligible influence on the activity (see Figure S6). A reductive treatment of the spent catalyst in a flow of 5%H_2/Ar for 1 h at 610 °C also proved to be ineffective in recovering the initial activity (see Figure S6). Based on the TGA analysis (see Figure 10), most of the deposited carbon species should have been depleted by the oxidative treatment, but the activity was essentially not affected. This result strongly suggests that carbon deposition was not responsible, at least not as the major factor, for the deactivation of Fe/ZSM-5 catalysts in the EDH reaction. In addition, this result also proved that the carbon deposits did not contribute, at least not significantly, to the steady-state activity of Fe/ZSM-5 catalysts, although some studies in the literature have suggested that carbon species formed on the catalyst surface could catalyze the dehydrogenation reaction [34-35].

Apart from the carbon deposition, TEM characterization of the used catalysts also indicated that sintering or growth of Fe nanoparticles occurred during the reaction. Apparently, it is not possible to re-disperse the active Fe species by simply oxidative or reductive treatment. Therefore, we believe that the deactivation of Fe/ZSM-5 catalysts in the EDH reaction was mainly caused by the sintering of Fe nanoparticles, which led to reduced number of active sites. The sintering probably resulted from the relatively high reaction temperature and/or reaction-induced migration of Fe species [36-38], the rate of which should be fairly slow as reflected by the smooth decline of the activity.

Note that the changes in the zeolite structure may also play a role in the relatively faster deactivation of the higher-loading Fe/ZSM-5 catalyst. The XPS analysis revealed that there was a significant decrease of Si/Al ratio from 20 to 10 for 10Fe/ZSM-5 after reaction, whereas the ratio on the other two catalysts only slightly decreased from 18 to 16 (see Table 2). Meanwhile, the weakened diffraction peak intensities in the XRD pattern of 10Fe/ZSM-5 also suggested that the crystalline structure of the ZSM-5 zeolite became less intact (see Figure 7). Accordingly, it may be deduced that the strong interaction between Fe oxides and the zeolite support might lead to the dealumination of the zeolite framework under EDH reaction conditions, especially at high Fe loading level, which would be detrimental for the activity of the Fe/ZSM-5 catalyst in view of the much inferior activity of Fe/Al_2O_3 catalyst (see Figure 1).

5. CONCLUSION

We have shown that iron supported on HZSM-5 zeolite can be used as efficient catalysts for the non-oxidative dehydrogenation reaction of ethane to ethylene. The iron-based catalysts exhibited the best stability and the highest steady-state activity towards ethylene production under the same reaction conditions, compared with various metal or metal oxide catalysts. The zeolite support proves to be the key to achieve optimal activity of iron catalysts, in view of its much higher ethane conversion than that on conventional γ-Al_2O_3 support. The activity of the Fe/ZSM-5 catalysts can be effectively enhanced by increasing the iron loading. Most prominently, the catalyst showed excellent stability with an activity loss of ≤40% after 15 hours of reaction. In addition, the production rate of ethylene on the Fe/ZSM-5 catalyst can be further enhanced by lowering the total flow rate as well as by increasing the concentration of ethane in the feed gas. The characterization results demonstrated that raising the Fe loading led to the

formation of larger Fe particle size. Based on the XRD, XPS, and DFT calculation results, both metallic and carburized iron are suggested to be the active sites for the EDH reaction, with the latter being more selective toward ethylene formation. The deactivation of the Fe/ZSM-5 catalysts was mainly attributed to the sintering or aggregation of Fe clusters under reaction conditions rather than the deposition of carbon. From a practical point of view, a strategy would need to be developed, if possible, to either re-disperse the Fe species or to prevent the aggregation of active Fe species by strengthening the interaction between the active Fe species and the surface of zeolite support.

Acknowledgement This work was supported by the U.S. Department of Energy (USDOE), Office of Energy Efficiency and Renewable Energy (EERE), Advanced Manufacturing Office (AMO) R&D Projects Emerging Research Exploration, and Idaho National Laboratory Directed Research and Development Program under DOE Idaho Operations Office under contract no. DE-AC07-05ID14517. The computing work was performed on the Beocat Research Cluster at Kansas State University, which is funded in part by NSF grants CHE-1726332, CNS-1006860, EPS-1006860, and EPS-0919443.

References

(1) Bhasin, M.; McCain, J.; Vora, B.; Imai, T.; Pujado, P., Dehydrogenation and oxydehydrogenation of paraffins to olefins. Applied Catalysis A: General 2001, 221 (1-2), 397-419.

(2) Sanfilippo, D.; Miracca, I., Dehydrogenation of paraffins: synergies between catalyst design and reactor engineering. Catalysis Today 2006, 111 (1-2), 133-139.

(3) Sattler, J. J.; Ruiz-Martinez, J.; Santillan-Jimenez, E.; Weckhuysen, B. M., Catalytic dehydrogenation of light alkanes on metals and metal oxides. Chemical reviews 2014, 114 (20), 10613-10653.

(4) Galvita, V.; Siddiqi, G.; Sun, P.; Bell, A. T., Ethane dehydrogenation on Pt/Mg (Al) O and PtSn/Mg (Al) O catalysts. Journal of Catalysis 2010, 271 (2), 209-219.

(5) Siddiqi, G.; Sun, P.; Galvita, V.; Bell, A. T., Catalyst performance of novel Pt/Mg (Ga)(Al) O catalysts for alkane dehydrogenation. Journal of Catalysis 2010, 274 (2), 200-206.

(6) Sun, P.; Siddiqi, G.; Chi, M.; Bell, A. T., Synthesis and characterization of a new catalyst Pt/Mg (Ga)(Al) O for alkane dehydrogenation. Journal of Catalysis 2010, 274 (2), 192-199.

(7) Sun, P.; Siddiqi, G.; Vining, W. C.; Chi, M.; Bell, A. T., Novel Pt/Mg (In)(Al) O catalysts for ethane and propane dehydrogenation. Journal of catalysis 2011, 282 (1), 165-174.

(8) Chen, H.; Li, L.; Hu, J., Upgrading of stranded gas via non-oxidative conversion processes. Catalysis Today 2018, 310, 94-97.

(9) Xiong, H.; Lin, S.; Goetze, J.; Pletcher, P.; Guo, H.; Kovarik, L.; Artyushkova, K.; Weckhuysen, B. M.; Datye, A. K., Thermally Stable and Regenerable Platinum─Tin Clusters for Propane Dehydrogenation Prepared by Atom Trapping on Ceria. Angewandte Chemie International Edition 2017, 56 (31), 8986-8991.

(10) Shao, C.-T.; Lang, W.-Z.; Yan, X.; Guo, Y.-J., Catalytic performance of gallium oxide based-catalysts for the propane dehydrogenation reaction: effects of support and loading amount. RSC Advances 2017, 7 (8), 4710-4723.

(11) De Cola, P. L.; Gläser, R.; Weitkamp, J., Non-oxidative propane dehydrogenation over Pt─Zn-containing zeolites. Applied Catalysis A: General 2006, 306, 85-97.

(12) Schreiber, M. W.; Plaisance, C. P.; Baumgärtl, M.; Reuter, K.; Jentys, A.; Bermejo-Deval, R.; Lercher, J. A., Lewis─Brønsted Acid Pairs in Ga/H-ZSM-5 To Catalyze Dehydrogenation of Light Alkanes. Journal of the American Chemical Society 2018, 140 (14), 4849-4859.

(13) Sokolov, S.; Stoyanova, M.; Rodemerck, U.; Linke, D.; Kondratenko, E. V., Comparative study of propane dehydrogenation over V-, Cr-, and Pt-based catalysts: Time on-stream behavior and origins of deactivation. Journal of catalysis 2012, 293, 67-75.

(14) Zhao, Z. J.; Wu, T.; Xiong, C.; Sun, G.; Mu, R.; Zeng, L.; Gong, J., Hydroxyl-Mediated Non-oxidative Propane Dehydrogenation over VOx/γ-Al2O3 Catalysts with Improved Stability. Angewandte Chemie International Edition 2018, 57 (23), 6791-6795.
(15) Mitchell, P.; Wass, S., Propane dehydrogenation over molybdenum hydrotalcite catalysts. Applied Catalysis A: General 2002, 225 (1-2), 153-165.
(16) Schweitzer, N. M.; Hu, B.; Das, U.; Kim, H.; Greeley, J.; Curtiss, L. A.; Stair, P. C.; Miller, J. T.; Hock, A. S., Propylene hydrogenation and propane dehydrogenation by a single-site Zn2+ on silica catalyst. Acs Catalysis 2014, 4 (4), 1091-1098.
(17) Camacho-Bunquin, J.; Aich, P.; Ferrandon, M.; Das, U.; Dogan, F.; Curtiss, L. A.; Miller, J. T.; Marshall, C. L.; Hock, A. S.; Stair, P. C., Single-site zinc on silica catalysts for propylene hydrogenation and propane dehydrogenation: Synthesis and reactivity evaluation using an integrated atomic layer deposition-catalysis instrument. Journal of Catalysis 2017, 345, 170-182.
(18) Cybulskis, V. J.; Bukowski, B. C.; Tseng, H.-T.; Gallagher, J. R.; Wu, Z.; Wegener, E.; Kropf, A. J.; Ravel, B.; Ribeiro, F. H.; Greeley, J., Zinc Promotion of Platinum for Catalytic Light Alkane Dehydrogenation: Insights into Geometric and Electronic Effects. ACS Catalysis 2017, 7 (6), 4173-4181.
(19) Virnovskaia, A.; Rytter, E.; Olsbye, U., Kinetic and isotopic study of ethane dehydrogenation over a semicommercial Pt, Sn/Mg (Al) O catalyst. Industrial & Engineering Chemistry Research 2008, 47 (19), 7167-7177.
(20) Hu, B.; Schweitzer, N. M.; Zhang, G.; Kraft, S. J.; Childers, D. J.; Lanci, M. P.; Miller, J. T.; Hock, A. S., Isolated FeII on silica as a selective propane dehydrogenation catalyst. Acs Catalysis 2015, 5 (6), 3494-3503.
(21) Bandiera, J.; Taârit, Y. B., Ethane conversion: Kinetic evidence for the competition of consecutive steps for the same active centre. Applied Catalysis A: General 1997, 152 (1), 43-51.
(22) Barthos, R.; Széchenyi, A.; Solymosi, F., Decomposition and aromatization of ethanol on ZSM-based catalysts. The Journal of Physical Chemistry B 2006, 110 (43), 21816-21825.
(23) Iwamoto, M.; Kosugi, Y., Highly selective conversion of ethene to propene and butenes on nickel ion-loaded mesoporous silica catalysts. The Journal of Physical Chemistry C 2007, 111 (1), 13-15.
(24) Tan, P., Active phase, catalytic activity, and induction period of Fe/zeolite material in nonoxidative aromatization of methane. Journal of Catalysis 2016, 338, 21-29.
(25) Sacco Jr, A.; Thacker, P.; Chang, T. N.; Chiang, A. T., The initiation and growth of filamentous carbon from α-iron in H2, CH4, H2O, CO2, and CO gas mixtures. Journal of Catalysis 1984, 85 (1), 224-236.
(26) Takenaka, S.; Serizawa, M.; Otsuka, K., Formation of filamentous carbons over supported Fe catalysts through methane decomposition. Journal of Catalysis 2004, 222 (2), 520-531.
(27) Bhargava, G.; Gouzman, I.; Chun, C.; Ramanarayanan, T.; Bernasek, S., Characterization of the "native" surface thin film on pure polycrystalline iron: A high resolution XPS and TEM study. Applied Surface Science 2007, 253 (9), 4322-4329.
(28) Biesinger, M. C.; Payne, B. P.; Grosvenor, A. P.; Lau, L. W.; Gerson, A. R.; Smart, R. S. C., Resolving surface chemical states in XPS analysis of first row transition metals, oxides and hydroxides: Cr, Mn, Fe, Co and Ni. Applied Surface Science 2011, 257 (7), 2717-2730.
(29) Wilson, D.; Langell, M., XPS analysis of oleylamine/oleic acid capped Fe3O4 nanoparticles as a function of temperature. Applied Surface Science 2014, 303, 6-13.

(30) Kuivila, C.; Butt, J.; Stair, P., Characterization of surface species on iron synthesis catalysts by X-ray photoelectron spectroscopy. Applied surface science 1988, 32 (1-2), 99-121.
(31) Hofmann, S.; Sharma, R.; Ducati, C.; Du, G.; Mattevi, C.; Cepek, C.; Cantoro, M.; Pisana, S.; Parvez, A.; Cervantes-Sodi, F., In situ observations of catalyst dynamics during surface-bound carbon nanotube nucleation. Nano letters 2007, 7 (3), 602-608.
(32) Panzner, G.; Diekmann, W., The bonding state of carbon segregated to α-iron surfaces and on iron carbide surfaces studied by electron spectroscopy. Surface science 1985, 160 (1), 253-270.
(33) Wiltner, A.; Linsmeier, C., Formation of endothermic carbides on iron and nickel. physica status solidi (a) 2004, 201 (5), 881-887.
(34) McGregor, J.; Huang, Z.; Parrott, E. P.; Zeitler, J. A.; Nguyen, K. L.; Rawson, J. M.; Carley, A.; Hansen, T. W.; Tessonnier, J.-P.; Su, D. S., Active coke: Carbonaceous materials as catalysts for alkane dehydrogenation. Journal of Catalysis 2010, 269 (2), 329-339.
(35) Sun, Y.; Wu, Y.; Tao, L.; Shan, H.; Wang, G.; Li, C., Effect of pre-reduction on the performance of Fe2O3/Al2O3 catalysts in dehydrogenation of propane. Journal of Molecular Catalysis A: Chemical 2015, 397, 120-126.
(36) Borry, R. W.; Kim, Y. H.; Huffsmith, A.; Reimer, J. A.; Iglesia, E., Structure and density of Mo and acid sites in Mo-exchanged H-ZSM5 catalysts for nonoxidative methane conversion. The Journal of Physical Chemistry B 1999, 103 (28), 5787-5796.
(37) Pérez-Ramírez, J.; Groen, J.; Brückner, A.; Kumar, M. S.; Bentrup, U.; Debbagh, M.; Villaescusa, L., Evolution of isomorphously substituted iron zeolites during activation: comparison of Fe-beta and Fe-ZSM-5. Journal of Catalysis 2005, 232 (2), 318-334.
(38) Yun, J. H.; Lobo, R. F., Catalytic dehydrogenation of propane over iron-silicate zeolites. Journal of Catalysis 2014, 312, 263-270.